Aerosol Science and Technology, 37:804–817, 2003

ISSN: 0278-6826 print / 1521-7388 online
DOI: 10.1080/02786820390223963

Development and Validation of a Simple Numerical Model for Estimating Workplace Aerosol Size Distribution Evolution Through Coagulation, Settling, and Diffusion

Andrew D. Maynard and Anthony T. Zimmer
National Institute for Occupational Safety and Health, Cincinnati, Ohio

Recent research has indicated that the toxicity of inhaled ultrafine particles may be associated with the size of discrete particles deposited in the lungs. However, it has been speculated that in some occupational settings rapid coagulation will lead to relatively low exposures to discrete ultrafine particles. Investigation of likely occupational exposures to ultrafine particles following the generation of aerosols with complex size distributions is most appropriately addressed using validated numerical models. A numerical model has been developed to estimate the size-distribution time-evolution of compact and fractal-like aerosols within workplaces resulting from coagulation, diffusional deposition, and gravitational settling. Good agreement has been shown with an analytical solution to lognormal aerosol evolution, indicating good compatibility with previously published models. Validation using experimental data shows reasonable agreement when assuming spherical particles and coalescence on coagulation. Assuming the formation of fractal-like particles within a range of diameters led to good agreement between modeled and experimental data. The model appears well suited to estimating the relationship between the size distribution of emitted well-mixed ultrafine aerosols, and the aerosol that is ultimately inhaled where diffusion loses are small.

INTRODUCTION

Occupational aerosol exposure has traditionally been characterized by the mass concentration of particles within well-defined size ranges (CEN 1993; ISO 1995). However, recent research has indicated that for a number of low-solubility materials the number, size, and surface area of particles depositing in the lungs may all play a significant role in determining adverse health effects (Donaldson et al. 2000; Oberdörster 2000). Much of the resulting discussion has focused on ultrafine particles—nominally particles with a diameter smaller than 100 nm. For instance, research using polystyrene latex, PTFE, and TiO_2 particles has indicated lung deposition of ultrafine particles leads to a greater biological response than a similar mass of much larger particles (Oberdörster 2000). It has been suggested that the observed response is due to the increased available surface area associated with the ultrafine particles. An alternative hypothesis is that biological response is associated with particle number, possibly due to particle penetration through the interstitium into the bloodstream (Seaton et al. 1995; Nemmar et al. 2002). However, this hypothesis assumes that a substantial number of discrete ultrafine particles will deposit in the lungs following exposure. In many workplaces the number concentration of generated ultrafines is likely to reach sufficiently high concentrations to lead to rapid coagulation: In this case it may be hypothesized that the number concentration of particles below 100 nm being inhaled will be relatively small (Vincent and Clement 2000). Many workplaces also contain a range of aerosol sources, and it is conceivable that scavenging by large particles will lead to relatively few ultrafine particles being available for inhalation.

If the number concentration of discrete ultrafine particles entering the respiratory system is associated with toxicity, the persistence of particles within the ultrafine region between generation and inhalation becomes a critical factor in determining associated health risks. Estimates of ultrafine particle removal through coagulation from lognormal distributions are calculable analytically (Park et al. 1999). However, this approach is inappropriate where the distribution is not well characterized by a lognormal distribution, and in particular where it is multimodal. In the case of complex particle size distributions, numerical modeling provides a more appropriate method of estimating particle persistence through predicting the time-evolution of an aerosol. The use of numerical routines for modeling spatial and temporal aerosol dynamics is well established, and represented by an extensive literature (Kommu et al. (2002) provide an extensive review of methods). However, there is a lack of published information on validated models appropriate to understanding the temporal evolution of ultrafine aerosols in the workplace.

Received 23 July 2002; accepted 19 March 2003.
Address correspondence to Andrew D. Maynard, National Institute for Occupational Safety and Health, 4676 Columbia Parkway, Cincinnati, OH 45226, USA. E-mail: amaynard@cdc.gov

A relatively simple discrete numerical model has been developed to consider the temporal evolution of workplace-related aerosols extending into the ultrafine region. By assuming well-mixed "parcels" of aerosol travel between the source and the point of inhalation at a known velocity, the need for a spatial component within the model has been removed (it is assumed that the parcel volume is large compared to inhaled aerosol volume). The model is further simplified by restricting it to physical processes assumed to dominate the behavior of ultrafine particles released into a workplace environment—these being generation, coagulation, and deposition through settling and diffusion. No account has been made of nucleation and condensation, restricting the model to the point beyond which these processes become secondary to coagulation and deposition processes. Validation of the model has been carried out using an aerosol generated during high speed grinding, thus representing a multimodal occupational aerosol spanning several orders of particle diameter (Zimmer and Maynard 2002). The model was developed and run within the software package Mathematica® (Wolfram Research Inc., Champagne, IL).

MODEL

Coagulation

Smoluchowski theory (Smoluchowski 1917) describing the thermal coagulation of spherical particles in an initially monodisperse distribution has been used extensively and effectively as the basis for predicting coagulation-mediated size distribution evolution. Extending the theory to a polydisperse distribution gives the change in concentration of particles with mass m with time as

$$\frac{dn(m)}{dt} = \frac{1}{2}\int_0^m n(m_1)K(m_1, m-m_1)n(m-m_1)dm_1 - n(m)\int_0^\infty K(m, m_1)n(m_1)dm_1 \quad [1]$$

(Fuchs 1964). K is the coagulation coefficient describing the probability of coagulation between particles of mass m and m_1. For particles in the continuum region coagulation coefficient, K_0 is given by the standard expression

$$K_0(m, m_1) = 4\pi\left(\frac{d(m)+d(m_1)}{2}\right)\left(\frac{D(m)+D(m_1)}{2}\right), \quad [2]$$

where $d(m)$ is the diameter of a particle with mass m, and $D(m)$ is the diffusion coefficient of the particle.

As particle size enters the free molecular regime, assumptions leading to Equation (2) begin to break down. The Fuchs correction factor β extends the usefulness of Equation (2) through the transition regime into the free molecular regime, giving the coagulation coefficient K as

$$K = \beta K_0, \quad [3]$$

where

$$\beta = \left(\frac{d}{d+\delta} + \frac{\pi\lambda_p}{\sqrt{2}d}\right)^{-1} \quad [4]$$

λ_p is the particle mean free path. The factor δ is given by

$$\delta = \sqrt{2}\left\{\frac{1}{3d\lambda_p}\left[(d+\lambda_p)^3 - \left(d^2+\lambda_p^2\right)^{\frac{3}{2}}\right] - d\right\} \quad [5]$$

(Fuchs 1964). Equations (1) and (3) allow coagulation to be modeled between particles of a few nanometers in diameter to tens of micrometers in diameter and are well suited to numerical modeling.

Loss Rate

The rate of particle loss through gravitational settling assuming continuous mixing may be expressed as

$$\left.\frac{dn(m)}{dt}\right|_{settling} = -\frac{n(m)v_{ts}}{h}, \quad [6]$$

where h is a characteristic height of the modeled system and v_{ts} is the particle settling velocity. Diffusional losses are more complex to include. In an open environment it may be assumed that equivalent cells surround the aerosol cell being modeled, and thus the outward diffusional flux is matched by an equivalent inward flux. However, where the cell is bounded by solid surfaces, some account needs to be taken of diffusional losses to these surfaces. Assuming continuous mixing of the aerosol, the rate of particle loss through diffusion is given as

$$\left.\frac{dn(m)}{dt}\right|_{\text{wall losses}} = -\frac{AnD}{V\delta_{diff}}, \quad [7]$$

where A is the total surface area of deposition surfaces bounding the aerosol, V the bounded aerosol volume, and δ_{diff} the diffusion boundary layer depth at the surfaces. δ_{diff} is a function of particle diameter and air movement at the boundary and is not simply represented analytically. For complex geometries there is interaction between gravitational and diffusional deposition, and Equations (6) and (7) have been found to be inadequate in representing deposition rates. (Crump et al. 1983). However, for rectangular enclosures with vertical walls their use is appropriate (Crump and Seinfeld 1981). Wells and Chamberlain (1967) have shown δ_{diff} to be proportional to $D^{1/3}$for simple geometries, while Crump and Seinfeld (1981) suggest it to be approximately proportional to $D^{1/2}$ in a cubic geometry. For this case an approximation of the diffusion layer depth may therefore be given by

$$\delta_{diff} = kD^{\beta}, \quad [8]$$

where k is an empirically determined constant that is dependent on the geometry and conditions being modeled. β is expected to lie between 1/2 and 1/3.

In the model it was assumed that the aerosol was at charge equilibrium, and that electrostatic forces would have a secondary influence over coagulation and deposition. These assumptions appeared to satisfy the model validation against the experimental data in this case. However, in some workplaces an extension of the model to include electrostatic effects would undoubtedly be advantageous.

Combining Equations (1), (6), and (7) and adding terms describing aerosol dilution and particle generation gives the rate of change of particle concentration with time as

$$\frac{dn(m)}{dt} = \frac{1}{2}\int_0^m n(m_1)K(m_1, m-m_1)n(m-m_1)dm_1 - n(m)\int_0^\infty K(m, m_1)n(m_1)dm_1 - \frac{n(m)v_{ts}}{h} - \frac{An(m)D}{V\delta_{diff}} - \Gamma n(m) + S, \quad [9]$$

where Γ is the fractional dilution rate and S is a source term.

Equation (9) is used as the basis of the numerical model described here. An initial aerosol size distribution is described in terms of a series of discrete particle mass bins, with the number of particles in each bin representing particle number concentration between the upper and lower bin limits. A geometric series is used to define the mass bin series at time $t = 0$.

$\frac{dn}{dt}|_{t=0}$ is initially calculated within the model for each bin using the geometric midpoint particle mass, and the discrete form of Equation (9). Using this approach directly, mass is not conserved. The formation rate of particles with mass m_k due to coagulation of particles with masses m_i and m_j is therefore adjusted to conserve mass using the relationship

$$\left.\frac{dn(m_k)}{dt}\right|_{\text{coag. growth, adjusted}} = \left.\frac{dn(m_k)}{dt}\right|_{\text{coag. growth}} \times \frac{m_i + m_j}{m_k} \quad [10]$$

(Gentry and Cheng 1996). Aerosol mass is subsequently conserved in the modeled evolving size distribution.

Time Progression

An initial estimate of number concentration at time $t + \Delta t$ is given by

$$n(t+\Delta t) = n(t) + \left.\frac{dn}{dt}\right|_t \times \Delta t. \quad [11]$$

This approximation is useful in estimating a suitable value of Δt, and is used within the model to estimate Δt such that no bin is depleted by more than 50%, or increased by 100%. Although these limits are arbitrary, they effectively reduce potentially catastrophic extrapolation errors associated with very large values of Δt. The implicit assumption of Equation (11) is that for a sufficiently small value of Δt higher order derivatives of $n(t)$ are insignificant. A more precise estimate of $n(t + \Delta t)$ can be made using a Taylor expansion:

$$n(t+\Delta t)_i = n(t) + \sum_{m=1}^{i} \frac{1}{m!}\left.\frac{d^m n}{dt^m}\right|_t \times \Delta t^m, \quad [12]$$

where i represents the ith estimate of $n(t + \Delta t)$, although calculating successive derivatives becomes increasingly computationally intensive. A computationally efficient solution is to iteratively improve estimates of the mean value of $\frac{dn}{dt}$ between t and $t + \Delta t$ using

$$n(t+\Delta t)_i = n(t) + \frac{\Delta t}{2}\left(\left.\frac{dn}{dt}\right|_t + \frac{d}{dt}n(t+\Delta t)_{i-1}\right). \quad [13]$$

Successive iterations of Equation (13) approximate to

$$n(t+\Delta t)_i = n(t) + \sum_{m=1}^{i} \frac{1}{2^{m-1}}\left.\frac{d^m n}{dt^m}\right|_t \times \Delta t^m. \quad [14]$$

Using Equation (14), estimates of $n(t + \Delta t)$ may be iteratively improved until

$$\sum_d n_{i+1}(t+\Delta t) - \sum_d n_i(t+\Delta t) \le n_{\text{lim}}, \quad [15]$$

where n_{lim} is a preset convergence point. Equation (14) initially approximates the Taylor expansion well, although ultimately it does not converge. However, it is not a precise representation of Equation (13), and in practice successive estimates of $n(t + \Delta t)$ were found to converge rapidly.

The model as described thus far is limited by the somewhat arbitrary constraints on the initial selection of Δt. A more reasonable approach is to select Δt to ensure that the difference between successive estimates of $n(t + \Delta t)_i$ are within acceptable bounds (defined by Δn_{min} and Δn_{max}).

If it is assumed that $n(t + \Delta t)$ is well represented by the first three terms of the Taylor expansion, then the difference between the first and second order estimates of $n(t + \Delta t)$, denoted $\Delta n_{1,2}$, is given by

$$\Delta n_{1,2} = \frac{1}{2}\frac{d^2 n}{dt^2}\Delta t^2. \quad [16]$$

By evaluating $\frac{d^2 n}{dt^2}$, Δt may be re-estimated to give $\Delta n_{1,2}$ within the preset bounds when it lies outside the range $\Delta n_{min} \rightarrow \Delta n_{max}$.

Using this method, the maximum value of Δt is still restricted to that which will lead to no bin being depleted by more than a set percentage to prevent negative number concentrations. This criterion becomes particularly restrictive as bins experiencing high negative values of $\frac{dn}{dt}$ are depleted to the point of containing negligible particles, resulting in the modeled size distribution evolution being dominated by bins that represent an insignificant fraction of the whole distribution. Selecting Δt to deplete these bins by exactly 100% would solve this problem. However, the

method used to iteratively improve the estimate of $n(t + \Delta t)$ cannot be guaranteed to lead to precisely 100% depletion in a key bin. The solution within the model is to merge bins together that contained restrictively small numbers of particles, ensuring that Δt remains within acceptable limits.

Adaptive Bin Widths—Bin Merging

Following the final estimation of $n(t + \Delta t)$, the value of Δt is estimated for each bin that will lead to 50% depletion after the next time step (based on the mean value of $\frac{dn}{dt}$ between t and $t + \Delta t$). Bins where Δt is less than a preset target value (Δt_{target}) are merged with neighboring bins. Resulting upper and lower bin limits are calculated to conserve particle number and mass. Three regimes for bin merging are identified: bins adjacent to and including the lowest bin in the series (low regime), bins adjacent to and including the highest bin (high regime), and bins or series of bins bordered by nontagged bins on either side (middle regime) (Figure 1). For each, a different merging algorithm is used.

Middle Regime. Following merging, the lower edge of the first bin (m_{j-1}) is equivalent to m_{i-1}, and the upper edge of the second bin (m_{j+1}) is equivalent to m_{i+2} (Figure 1). The particle number in each resulting bin is set to

$$\begin{aligned} n_{j-1} &= n_{i-1} + \frac{1}{2} n_i, \\ n_j &= n_{i+1} + \frac{1}{2} n_i. \end{aligned} \qquad [17]$$

The lower edge of the upper bin following merging (m_j) is calculated to conserve mass, giving

$$m_j = \left(\frac{n_{i-1}\sqrt{m_{i-1}m_i} + n_i\sqrt{m_i m_{i+1}} + n_{i+1}\sqrt{m_{i+1}m_{i+2}}}{n_{j-1}\sqrt{m_{i-1}} + n_j\sqrt{m_{i+2}}} \right)^2. \qquad [18]$$

Lower Regime. Following merging, the particle number in the resulting bin (n_j) is equal to

$$n_j = n_i + n_{i+1} \qquad [19]$$

(Figure 1). The upper edge of the resulting bin is set to be the same as the upper edge of the adjacent bin (m_{i+2}), giving the lower edge of the resulting bin (m_j) as

$$m_j = \left(\frac{n_i\sqrt{m_i m_{i+1}} + n_{i+1}\sqrt{m_{i+1}m_{i+2}}}{n_j\sqrt{m_{i+2}}} \right)^2. \qquad [20]$$

Upper Regime. Particle number in the merged bin (n_j) is given by

$$n_j = n_i + n_{i-1} \qquad [21]$$

(Figure 1). The lower edge of the resulting bin is set to be the same as the lower edge of the adjacent bin (m_{i-1}), giving the upper edge of the resulting bin (m_{j+1}) as

$$m_{j+1} = \left(\frac{n_{i-1}\sqrt{m_{i-1}m_i} + n_i\sqrt{m_i m_{i+1}}}{n_j\sqrt{m_{i-1}}} \right)^2. \qquad [22]$$

For each regime the above algorithms are sequentially repeated for each tagged bin.

Solid Particle Coagulation—Inclusion of Fractal Dimension

The model as described up to this point assumes spherical particles and coalescence on coagulation, and thus is only strictly applicable to liquid aerosols. Coagulation of solid particles tends to form fractal-like agglomerates, which exhibit a behavior that is associated with their structure. There is an extensive literature on the formation and behavior of fractal-like aerosol agglomerates (e.g., Forrest and Witten, Jr. 1979; Schmidt-Ott 1988; Hagenloch and Friedlander 1989; Jiang and Logan 1991; Rogak et al. 1993; Wu and Friedlander 1993; Baron et al. 2001). However, an approach to formulating a general numerical coagulation model spanning the free molecular regime to the continuum regime is not immediately clear. Brownian coagulation is largely governed by particle diffusional mobility and effective collision diameter. In the case of spherical particles, mobility diameter and collision diameter can be assumed to be similar. However, this assumption breaks down for fractal-like agglomerates. Hagenloch and Friedlander (1989) have proposed that

$$\frac{d_{cl}}{d_0} \approx N^{\alpha} \qquad [23]$$

for *Kn*udsen number $Kn > 1$, where d_{cl} is the particle collision diameter, d_0 the primary particle diameter, and N the number of primary particles in the agglomerate. $\alpha \rightarrow 0.45$ as $Kn \rightarrow \infty$ for a fractal dimension D_f of 2.5. Equation (23) may be approximated as

$$N = \left(\frac{d_f}{d_0} \right)^{D_f} \qquad [24]$$

(Rogak et al. 1993), where d_f is the agglomerate's outer diameter. If d_f is assumed to be equivalent to d_{cl}, Equation (24) leads to $\alpha = 0.4$ for $D_f = 2.5$—a close approximation to Hagenloch and Friedlander. If d_0 and primary particle density ρ are known for an agglomerate of mass m, N is calculable, and d_{cl} can be estimated from Equation (24) as

$$d_{cl} \approx d_f = d_0 N^{\frac{1}{D_f}}. \qquad [25]$$

The mobility diameter (d_m) of agglomerates with $D_f < 2$ has been shown to be equivalent to the equivalent-sphere projected-area diameter d_A (Rogak et al. 1993). For $D_f < 2$ most of the primary particles in an agglomerate are exposed, and the projected-area can be assumed to be equivalent to the orientation-averaged

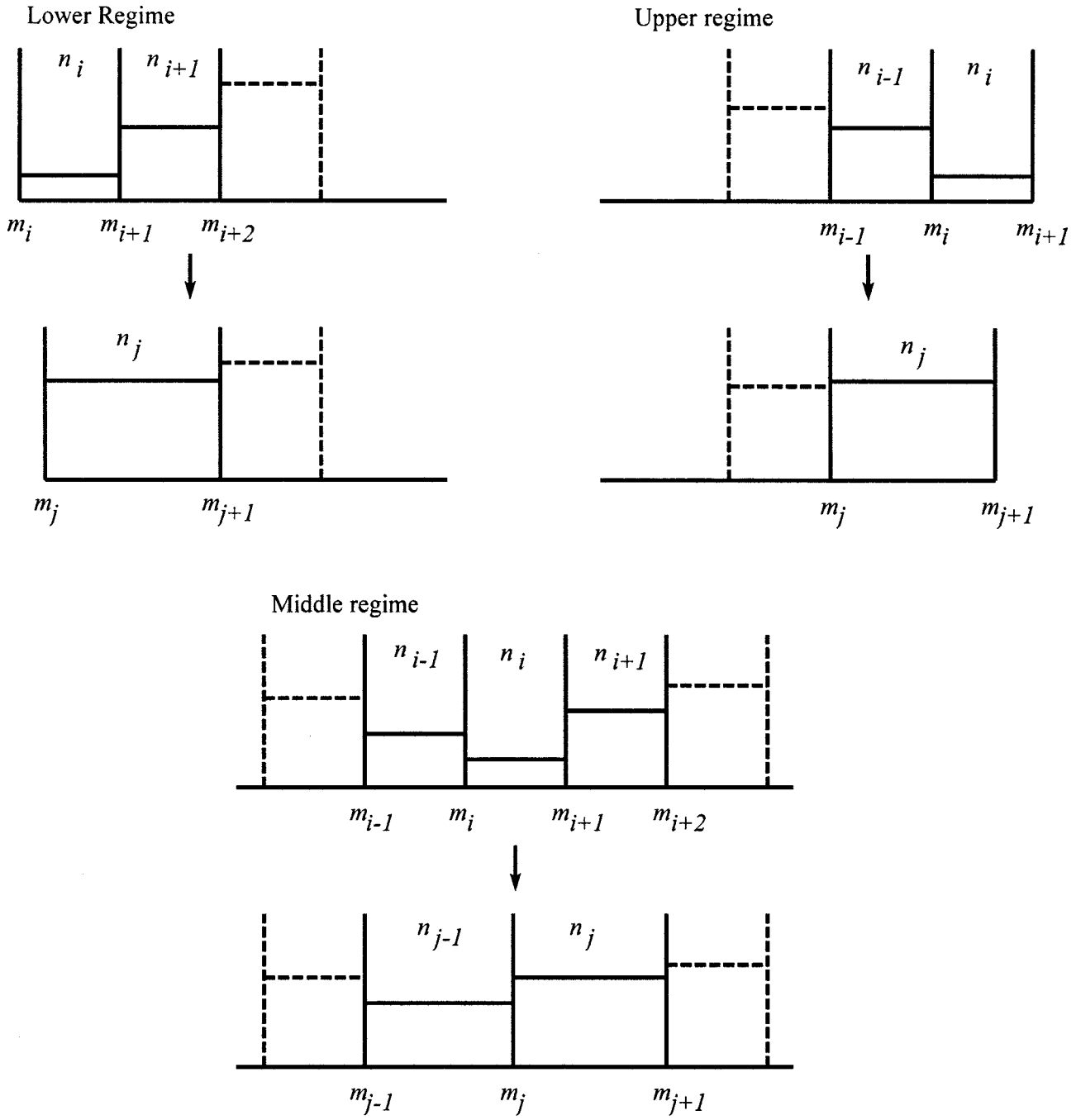

Figure 1. Schematic representation of algorithms used to merge mass bins when the particle number in a given bin is sufficiently low to lead to excessively short time steps.

area of a straight chain with the same N (Rogak et al. 1993). Thus

$$d_m \equiv d_A = \frac{d_0}{\sqrt{2}\pi}[(1+N)\pi^2 + 4(3\sqrt{3}-4)(N-1)]^{\frac{1}{2}}. \quad [26]$$

Coagulation coefficient K_0 is dependent on the relative diffusion rate between particles, and therefore may be effectively estimated using particle mobility diameter. However, the Fuchs correction factor β is estimated from the effective collision diameter of particles. Substituting d_m for d in Equation (2) and d_f for d in Equations (4) and (5) gives

$$K_{0,\,fractal}(m, m_1) = 4\pi\left(\frac{d_m(m) + d_m(m_1)}{2}\right)\left(\frac{D(m) + D(m_1)}{2}\right) \quad [27]$$

and

$$\beta_{fractal} = \left(\frac{d_f}{d_f + \delta_{fractal}} + \frac{\pi \lambda_p}{\sqrt{2} d_f} \right)^{-1},$$

$$\delta_{fractal} = \sqrt{2} \left\{ \frac{1}{3 d_f \lambda_p} \left[(d_f + \lambda_p)^3 - \left(d_f^2 + \lambda_p^2 \right)^{\frac{3}{2}} \right] - d_f \right\}, \quad [28]$$

with

$$K_{fractal} = \beta_{fractal} K_{0,\ fractal}, \quad [29]$$

allowing the coagulation model to be extended to fractal agglomerates with $D_f \leq 2$. The diffusion coefficient D in Equation (27) is clearly evaluated using d_m. Equation (29) becomes equivalent to Equation (3) for $D_f = 3$, allowing it to be used for compact and fractal-like particles. Wu and Friedlander (1993) have addressed the same problem starting from the free molecular regime expression for K, using similar assumptions. Their final expression for $K_{fractal}$ gives values that agree well with Equation (29). However, their expression is only of use for $Kn > 10$ and $D_f > 2$, and thus was not used within the numerical model.

While Equation (29) allows the growth of fractal-like aerosols to be modeled effectively, it is unrealistic to assume all particles within an aerosol will have the same fractal dimension. In the simplest terms, it may be assumed that particle morphology is driven by generation mechanism, with fine particles tending towards a fractal-like geometry, and coarse particles tending towards a compact geometry. This assumed tendency is incorporated into the model as a step function defining D_f—particles smaller than a limiting diameter (d_{limit}) are assumed to be fractal-like (when modeling solid particle behavior), while particles larger than d_{limit} are assumed to be spherical. Although this is an oversimplification, it allowed effective comparison with experimental data. The model also assumes that particles smaller than the primary particle size are spherical.

MODEL VALIDATION

Comparison with an Existing Analytical Model

Initial validation of the discrete numerical model was carried out against an analytical model describing the coagulation of lognormal aerosol size distributions for the entire particle

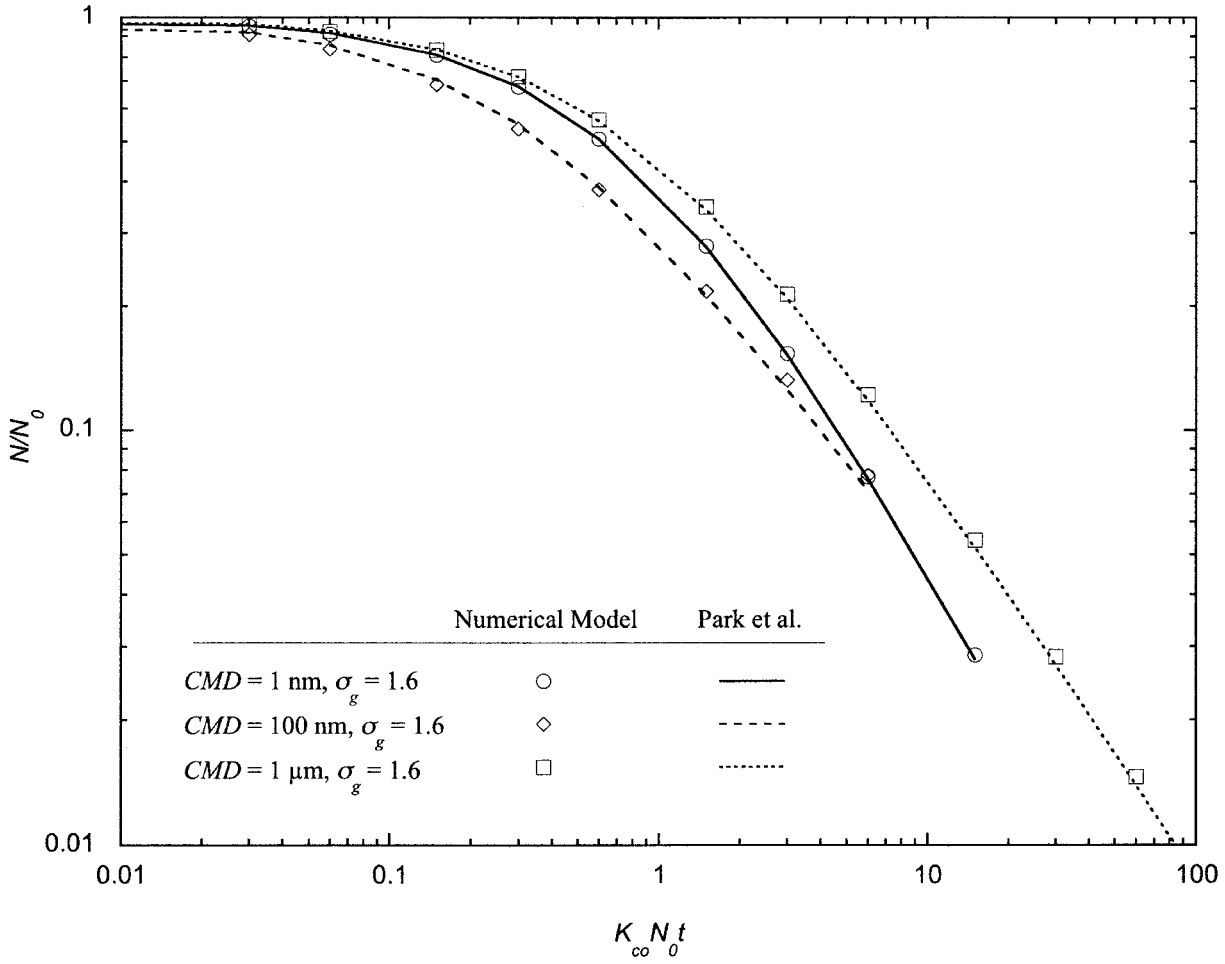

Figure 2. Plotting normalized particle number concentration versus dimensionless time for the analytical lognormal coagulation model of Park et al. (1999) and the numerical coagulation model. K_{co} is the coagulation coefficient in the continuum regime.

size range (Park et al. 1999). The Park et al. analytical model has been compared favorably with both sectional and discrete numerical models (Otto et al. 1999), making it particularly suitable for validating new code. Comparisons were made between the time-evolution of three lognormal distributions, representing coagulation in the free-molecular regime (Count Median Diameter (CMD)) = 1 nm, the transition regime (CMD = 100 nm), and the continuum regime (CMD = 1 μm). In each case the geometric standard deviation was 1.6, and the number concentration 10^{12} particles/m^3. The time-evolution of each distribution was modeled for between 20,000 s and 100,000 s in each case.

Figure 2 compares normalized number concentration against dimensionless time for each distribution. In each case very close agreement between the discrete numerical model and the analytical model is seen. Size distributions for the transition-regime aerosol are plotted in Figure 3 for each model. The discrete model appears to slightly underestimate number concentration close to the median diameter, and overestimate it towards the edges of the distribution. However this is most likely an artifact of using discrete size bins. Overall the agreement between both models is very close.

Validation Against Experimental Data

Experimental Method. Experimental validation of the numerical model was carried out by measuring the temporal size distribution evolution of polydisperse aerosols spanning over three decades of particle diameter. The aerosols were generated through high-speed grinding of a series of substrates—a method previously shown to generate particles from a few nanometers in diameter up to tens of micrometers in diameter (Zimmer and Maynard 2002).

The generation method used was identical to that described by Zimmer and Maynard. HEPA-filtered, particle-free air was pulled upward through a stainless steel chamber (approximately 1 m^3) (Figure 4). Prior to measurements, the HEPA-filtered air within the chamber was monitored using a condensation particle counter (CPC) (TSI Inc., Model 3022A, Shoreview, MN). When

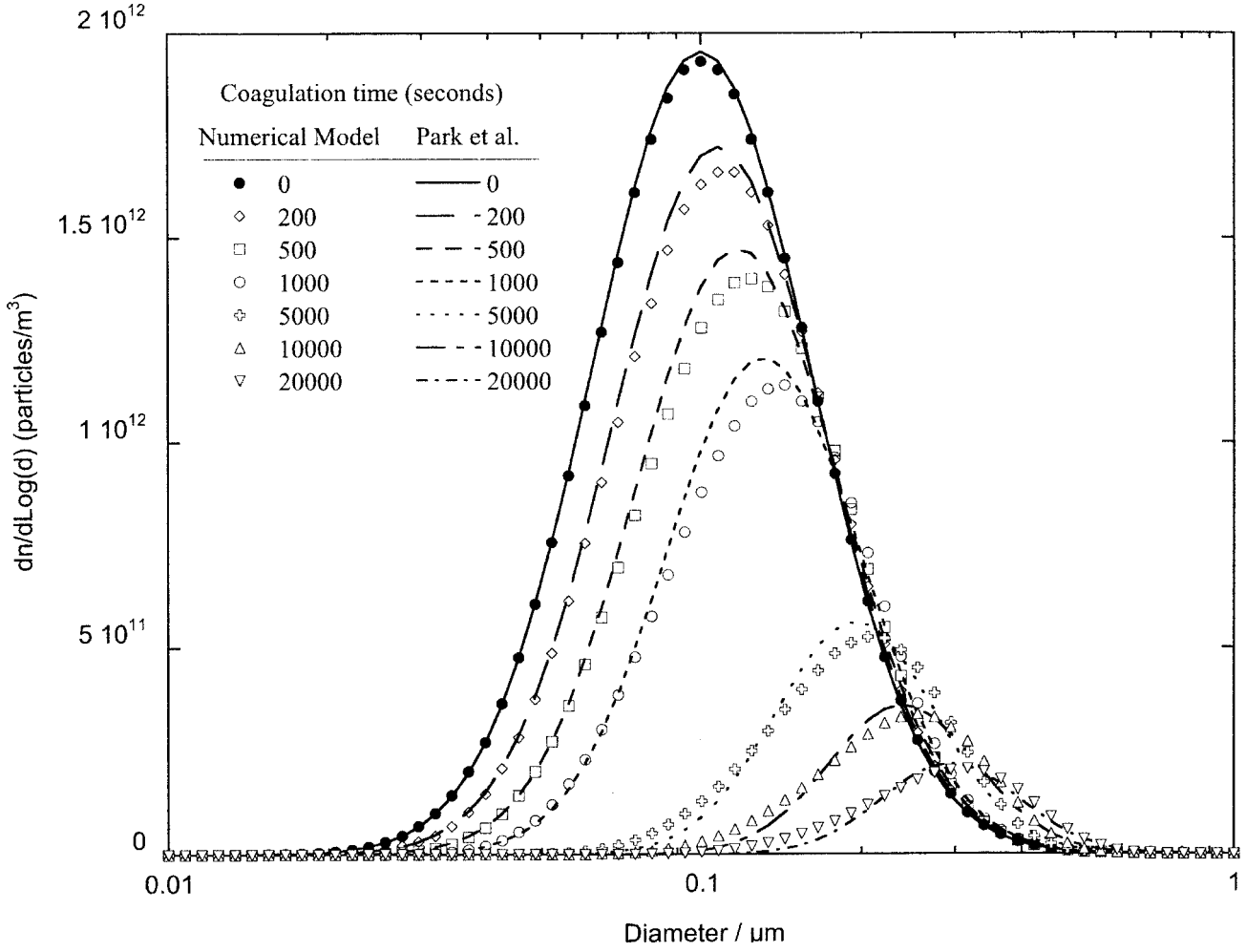

Figure 3. Comparison of the numerical model and the Park et al. (1999) analytical lognormal model for an initial lognormal aerosol distribution with *CMD* = 100 nm, $\sigma_g = 1.6$, and number concentration = 10^{12} particles/m^3.

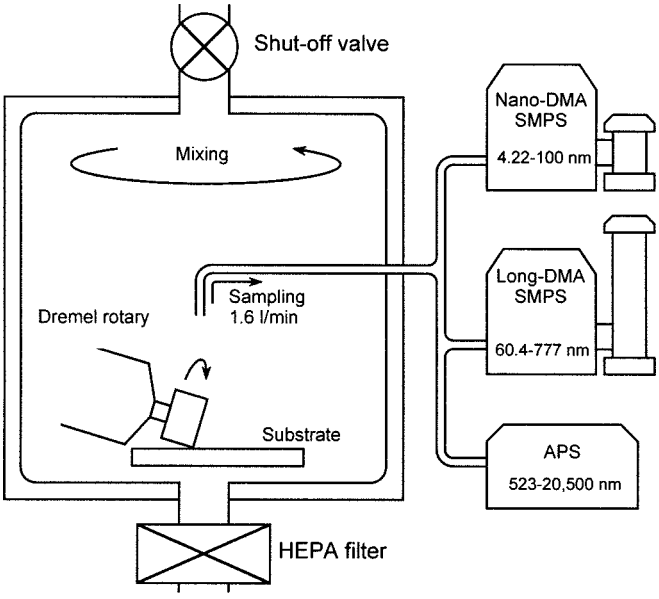

Figure 4. Schematic of the experimental aerosol generation and sampling system (not to scale).

the particle number concentration was reduced to a value of approximately 50×10^6 particles/m^3, the air flow was stopped, and the chamber sealed. Concentrations below this were not achievable due to some infiltration into the chamber. A small, tubeaxial fan (Pamotor, Model 8500C, Burlingame, CA), located within the base of the chamber, was used to create "stirred" conditions (CPC measurements validated that the fan did not represent a source of aerosols).

Grinding was carried out using a Dremel Multipro^{TM} (Model 395, Racine, WI), a variable-speed tool with rotational speeds that can be varied from 5000 to 30000 revolutions per minute (rpm). A cylindrical aluminum oxide grinding wheel was selected for these experiments. The rotational speed of the grinding wheel set at approximately 20,000 rpm in each case. Grinding was accomplished such that the cylindrical wheel was placed normal to the substrate with a constant applied force of 3.96 N. The substrates selected for grinding included aluminum, polytetrafluoroethylene (PTFE), and granite.

Aerosol samples were collected from the chamber at a position located directly above the grinding operation (height = 0.15 m). The aerosol-laden air collected from the chamber was split and directed to one of three aerosol instruments operated in parallel. The smallest particles (4.22 nm $< d_m <$ 100 nm) were characterized using a scanning mobility particle sizer (SMPS) configured with a nano differential mobility analyzer (DMA) (TSI Inc., an Electrostatic Classifier, Model 3080, using a Nano Differential Mobility Analyzer, Model 3085, and a Condensation Particle Counter (CPC), Model 3022A, St. Paul, MN). Larger particles (60.4 nm $< d_m <$ 777 nm) were characterized using a SMPS configured with a long DMA (TSI Inc., DMA Model 3934 and CPC Model 3022A, St. Paul, MN). The largest particles (523 nm < aerodynamic diameter $d_{ae} < 20.5\mu$m) were characterized using an aerodynamic particle sizer (APS) (TSI Inc., Model 3320). Particle number concentrations detected by each instrument were sufficiently low to lead to significant overload or coincidence errors. The overall sampling flow rate to the three instruments was 1.6 l/min. To minimize aerosol extraction from the chamber, instruments were disconnected from it between samples being taken. Rogak et al. (1993) have shown particle mobility diameter to agree well with equivalent-sphere projected-area diameter for fractal-like particles below 1 μm. The assumption was therefore made that the data from each SMPS could be interpreted in terms of particle equivalent-sphere projected-area diameter. Particles large enough to be sampled by the APS were assumed to arise predominantly through attrition, and have a compact morphology. APS aerosol size distributions were therefore transformed to particle number concentration versus equivalent sphere projected-area diameter assuming spherical particles with the same density as the bulk substrate material. The APS data were also corrected for sampling train losses between the chamber and the instrument inlet, and losses within the APS nozzle (Kinney and Pui 1995). Calculations indicated sampling train losses to each SMPS to be negligible.

Low concentration aerosols of PTFE and granite were generated to investigate particle deposition through diffusion and gravitational settling, in the absence of significant coagulation. In each case the substrate was ground for 10 s, and the aerosol allowed to fully mix within the chamber for 60 s. prior to sampling. Size distribution measurements were then taken at intervals over the next 2–4 h, with each measurement taking 200 s.

To increase the aerosol concentration sufficiently for coagulation to play a significant role, the aluminum substrate was ground continuously until a stable size distribution was obtained. At this point three consecutive distribution measurements were made over a period of 10 min to ensure the distribution was stable prior to starting the time series measurements. Although there were small variations in the distribution with time, these were considered insignificant. The average of the three initial measured distributions was taken to represent the aerosol size distribution at $t = 0$ s. Size distribution measurements were then taken at 500 s, 1500 s, and 4500 s following termination of grinding, with each sample lasting 200 s. Over the course of the sampling period, 5% of the air within the chamber was removed by the sampling instruments. Replenishment of sampled air with clean air during experimental measurements was modeled using the dilution term in Equation (9).

Comparison with Model. Experimental data for all substrates indicated very broad polydisperse distributions. Data from each instrument agreed well in the overlap regions, allowing a continuous distribution between 4 nm and 20 μm to be measured in each case.

With the low particle concentrations from the granite and PTFE substrates (total particle concentrations $<3\times10^{11}$ particles/m^3) it was assumed that diffusional losses and gravitational losses would dominate at small and large particle diameters,

respectively, allowing the validity of Equation (8) to be explored, and appropriate values of k, α, and h to be derived.

From Equation (7), if diffusional deposition is assumed to be the only removal mechanism, the number concentration of particles of diameter d_m is expected to vary as

$$n(d_m t) = n_0 e^{-\frac{AD}{V\delta}t}, \quad [30]$$

where n_0 is the number concentration at $t = 0$. Thus from Equation (8),

$$k = -\frac{AD^{1-\alpha}t}{V}\frac{1}{Ln(n/n_0)}. \quad [31]$$

Evaluating the data from grinding on granite between 5 nm and 20 nm at 440 s and 1440 s with $\alpha = 1/3$ led to a clear trend of increasing k with increasing diameter. Using $\alpha = 1/2$ led to no clear trend between k and particle diameter, and relatively little variance in the values of k obtained. $\alpha = 1/2$ was therefore used to model this particular aerosol containment geometry, giving $k = 0.050 \pm 0.005\ m^{\frac{1}{3}}s^{\frac{1}{3}}$. Evaluating the PTFE data resulted in a similar value of k.

Preliminary inspection of both the PTFE and granite data indicated that gravitational settling was not well represented by using the full chamber height for h in Equation (6). This was not surprising, as the mixing fan was positioned to ensure mixing in the lower half of the chamber. Changes in number concentration above 1 μm indicated that an effective height h of 0.25 m represented the experimental data well (based on gravitational settling rates). This was reasonable given the positioning of the circulation fan, the grinding tool, and the sample exit point within the chamber. Figures 5 through 7 confirm that using an effective height of 0.25 m allows measured size distributions above 1 μm to be modeled well.

Figure 5 shows the experimental versus modeled PTFE data. The experimental and modeled data for the granite substrate gave very similar results, and are thus not shown. Compact spherical particles and coalescence on coagulation were assumed. Modeled data for both substrates agreed well with experimental data up to 4500 s, indicating that the empirical values of δ and h are applicable to different aerosols under different conditions. At 13500 s there is considerable disagreement between the model and the PTFE data below 500 nm and some disagreement above

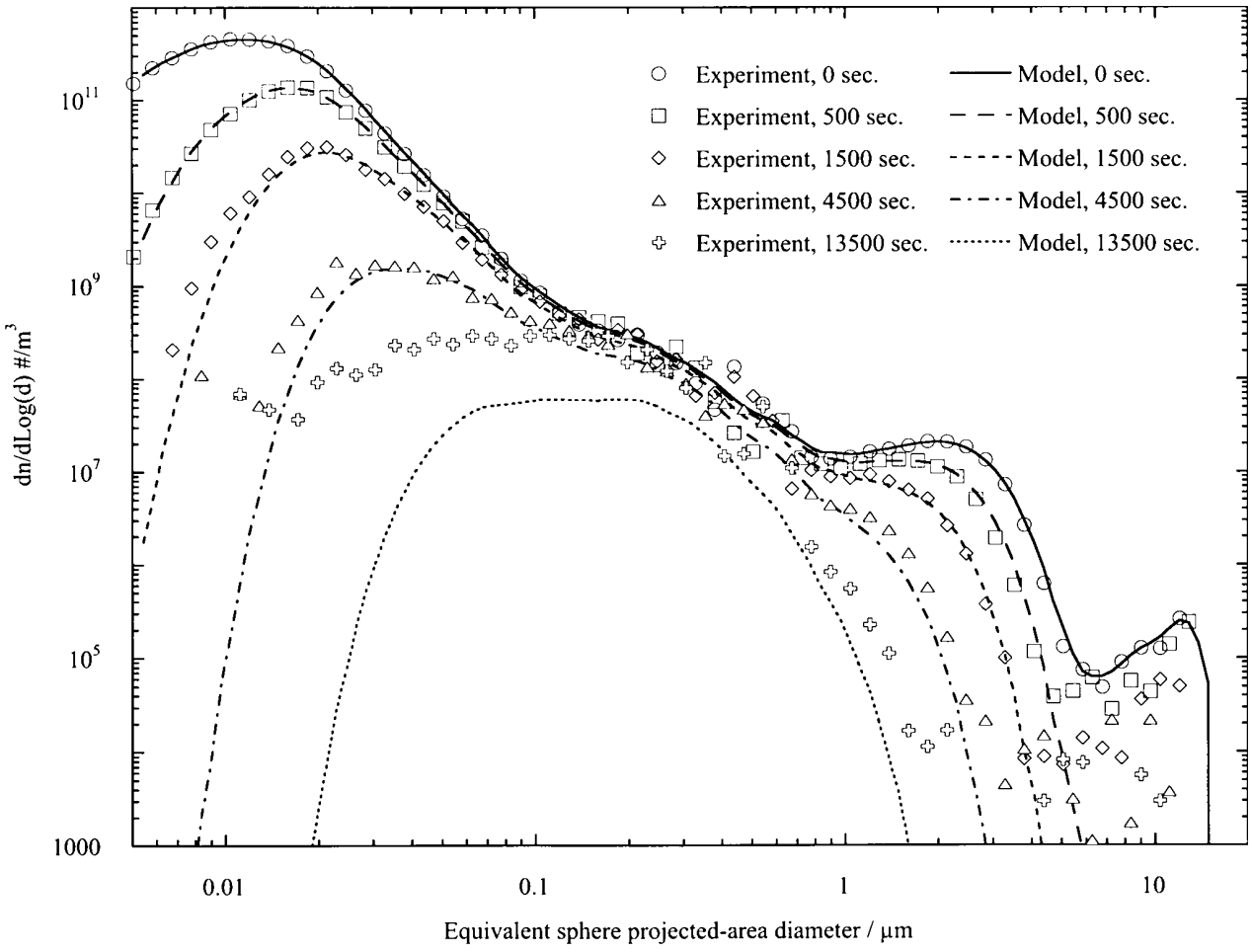

Figure 5. Comparison of experimental and modeled aerosol size distributions for PTFE grinding aerosol.

1 μm. At this measurement point the overall aerosol number concentration was approaching the achievable background concentration within the chamber. Further investigation confirmed that a degree of infiltration occurred with time into the chamber from the ambient aerosol, explaining the apparent divergence between model and experimental data. This nonquantifiable source is also a possible explanation for increasing divergence between the model and experimental data with time below 30 nm. Above 8 μm aerosol concentration was very low, leading to substantial experimental measurement errors, and it is unlikely that differences between the model and experimental data are significant.

The slightly higher aerosol concentration ($\sim 10^{12}$ particles/m^3) achievable with the aluminum substrate allowed the model to be compared with experimental data where coagulation was a significant mechanism. Unlike the experimental data from PTFE and granite, an initial measurement of the aluminum aerosol distribution was made before the grinding tool was switched off to provide the $t = 0$ size distribution. Figure 6 compares experimental and modeled size distributions at 500 s, 1500 s, and 4500 s. The model was run a number of times assuming a range of particle morphologies. As well as modeling the time-evolution of spherical particles ($D_f = 3$), open fractal-like agglomerates ($D_f = 1.7$) were modeled using primary particle diameters of $d_p = 10$ nm, 20 nm, 30 nm, and 50 nm, and $d_{limit} = 200$ nm and 500 nm (Figure 6b)—only data for $d_p = 20$ nm and 30 nm are shown for clarity. Size distributions for $d_p = 10$ nm lay below those for $d_p = 20$, and size distributions for $d_p = 50$ nm lay above those for $d_p = 30$ nm). Primary particle density was assumed to be that of bulk aluminum (2700 kg/m^3). The model was also run with coagulation switched off to allow the contribution of coagulation to the modeled data to be assessed (Figure 6a).

Agreement between experimental and modeled data above 1 μm is comparable with that for PTFE and granite, indicating that assuming compact particles above a set diameter is justified. With coagulation switched off the reduction in particle number concentration versus diameter at 500 s is increasingly underestimated below 70 nm, with the difference between experimental and modeled data being over a factor of 20 at 5 nm. Above 70 nm there is little difference seen when coagulation is included.

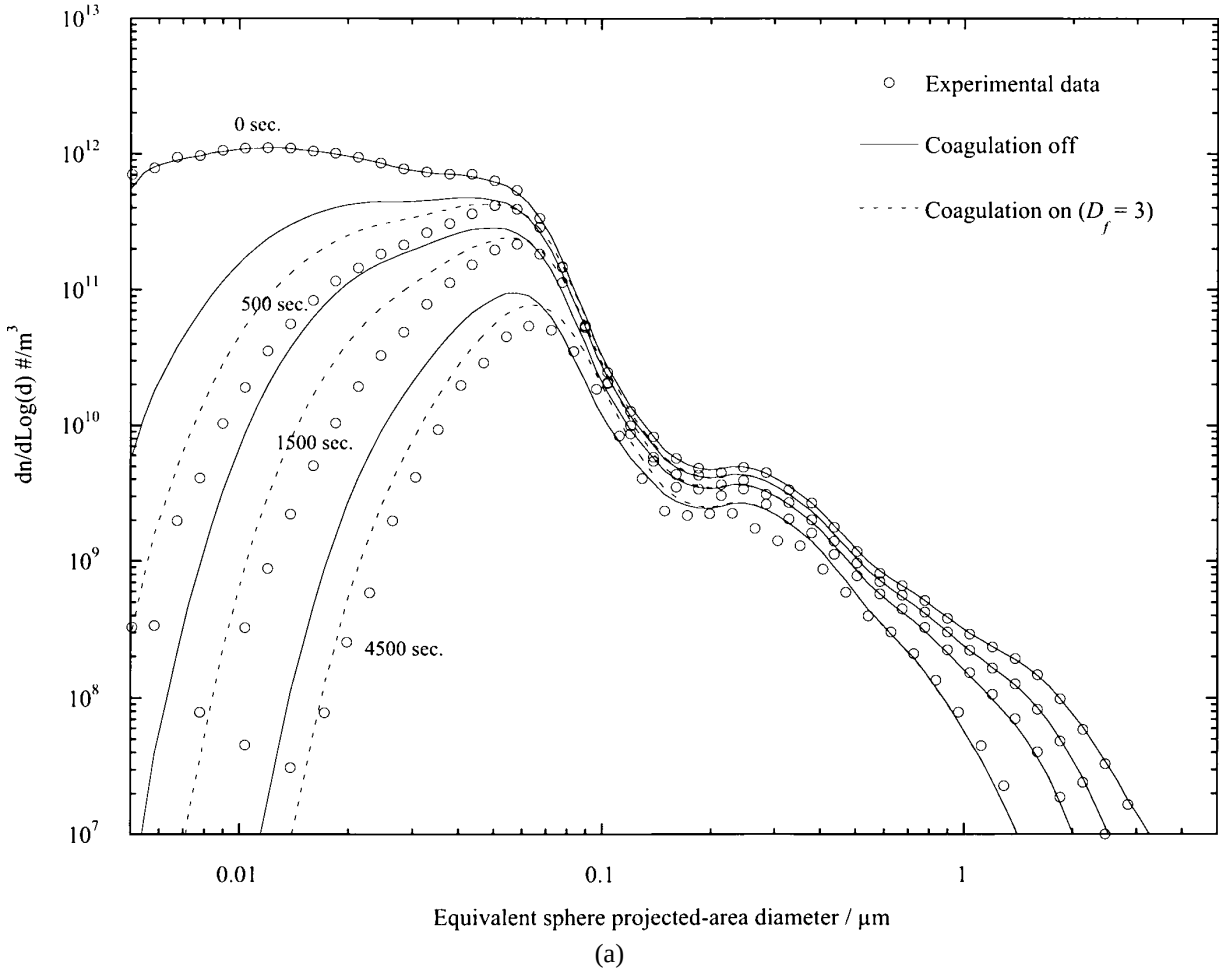

(a)

Figure 6. Experimental and modeled size distributions for aluminum aerosol. (a) Assuming spherical particles and coalescence on coagulation. Modeled data are shown with coagulation switched on and off in the model. (b) Assuming fractal particles with $D_f = 1.7$ within the range $d_p \leq d \leq d_{limit}$. *(Continued)*

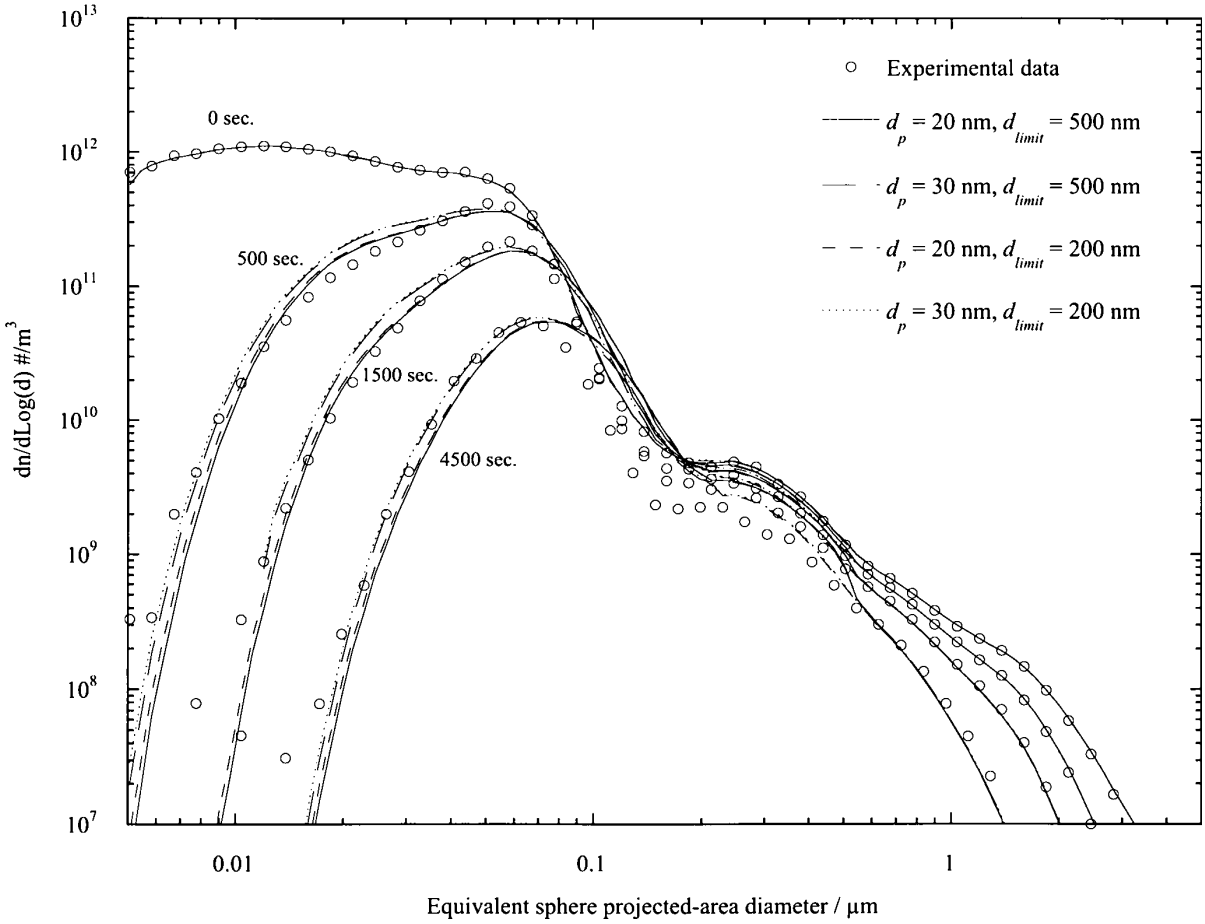

(b)

Figure 6. (Continued)

Including coagulation and assuming compact particles (and coalescence on coagulation) leads to better agreement between the model and experimental data. Divergence between experimental and modeled data below 20 nm becomes increasingly significant, although there is a trend towards better agreement below 6 nm.

Assuming the particles have a fractal-like structure results in substantially better agreement between modeled and experimental data. Assuming a primary particle diameter between 20 and 30 nm gives good agreement with experimental data below 50 nm. Discrepancies occur between around 50 nm and d_{limit}, indicating that the particle morphology model used is too crude to accurately represent behavior in this region. Imaging of aerosol particles in the Transmission Electron Microscope indicated a large number of single spherical particles below around 20 nm in diameter, with most particles above approximately 500 nm in diameter being single compact particles. Some open agglomerates of nanometer-sized primary particles were visible. However, quantitative analysis of their number concentration was not possible. From these observations of the particles the fractal/nonfractal model used would appear broadly appropriate. Discrepancies between experiment and model between d_p and d_{limit} may be attributable to the crudeness of assumptions on particle fractal dimension, although insufficient evidence was available to directly support this.

VARYING MODEL EVALUATION PARAMETERS

Computational time for explicit numerical coagulation models with fixed time steps is approximately proportional to N_{bin}^2, where N_{bin} is the number of mass bins used to describe the size distribution. As the dominant features in most distributions tend to scale with the log of diameter, using a geometric bin series is effective in describing distributions spanning diameters of several orders of magnitude, while keeping the total bin number within reasonable limits. However, significant savings can be made in computation time by further reducing the number of bins per decade used to represent the aerosol.

The influence on the number of mass bins per decade was qualitatively investigated using the aluminum grinding data assuming compact particles. The model was run using 14.068, 7.034, 3.517, and 1.759 bins per decade for particle mass (Table 1).

Table 1
Relative computation times as a function of n_{min} and the number of mass bins per decade for modeling aluminum aerosol evolution up to 4500 s

n_{lim} (%)	Mass bins per decade	Relative computation time
Reference model	7.034	1
10	7.034	0.031
5	7.034	0.018
2	7.034	0.022
1	7.034	0.029
0.5	7.034	0.060
0.2	7.034	0.075
0.1	7.034	0.090
1	14.068	0.15
1	3.517	0.00047
1	1.759	0.00017

In each case $\Delta n_{min} = 0.1 \times n_{lim}$, $\Delta n_{max} = 2 \times n_{lim}$.
The reference model used a fixed time step of 1 s.

Two other factors within the model that strongly influence computation time are the length of the time step Δt selected, and the convergence limit n_{lim} placed on successive estimates of $n(t + \Delta t)$. The influence of varying n_{lim}, and using a variable value of Δt as opposed to a fixed value, were qualitatively evaluated, again using the aluminum grinding data. n_{lim} was varied between 0.1% and 10%, with the lower and upper limits on Δn_{min} and Δn_{max} being set to $0.1 \times n_{lim}$ and $2 \times n_{lim}$, respectively, in each case. A set of reference distributions were generated using 7.034 mass bins per decade and a fixed time step $\Delta t = 1$ s. Table 1 compares the relative computation time for each model run, and the resulting size distributions are shown in Figure 7.

Figure 7a compares size distributions for $0.1\% \leq n_{lim} \leq 10\%$. In each case there is negligible difference between the distributions, and the reference distribution derived using a fixed time step. However, increases in computational efficiency are marked, with computation times decreasing by a factor of 50 when $n_{lim} = 5\%$, compared to the reference model (Table 1). Varying the number of bins per decade also led to negligibly small differences between distributions, although interpolation

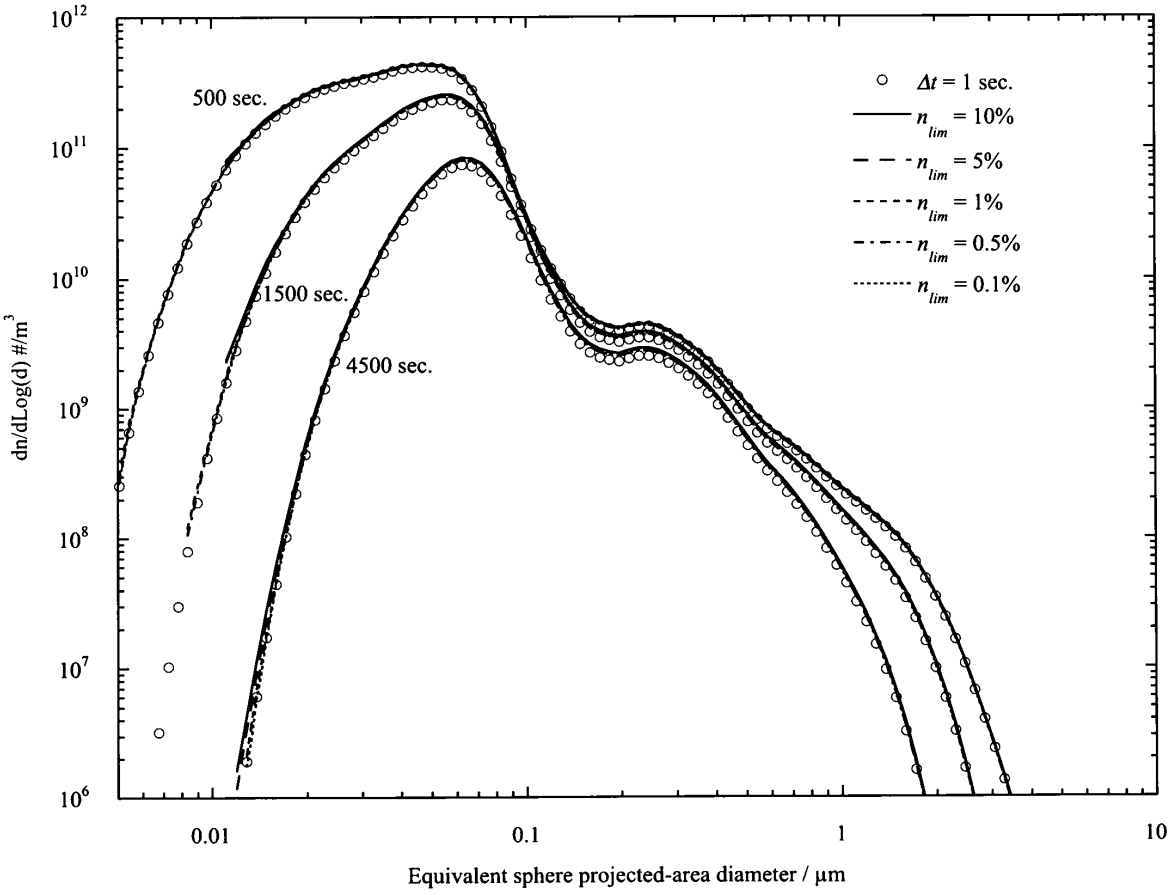

(a)

Figure 7. Modeled size distributions for aluminum between 500 s and 4500 s, varying n_{lim} and the number of mass bins per decade. Reference model distributions have been calculated with a fixed time step of 1 s, and linear extrapolation to $t + \Delta t$ (Equation (11)). (a) Varying n_{lim} between 10% and 0.1% (with 7.034 mass bins per decade). (b) Varying the number of mass bins between 1.759 and 14.068 bins per decade. *(Continued)*

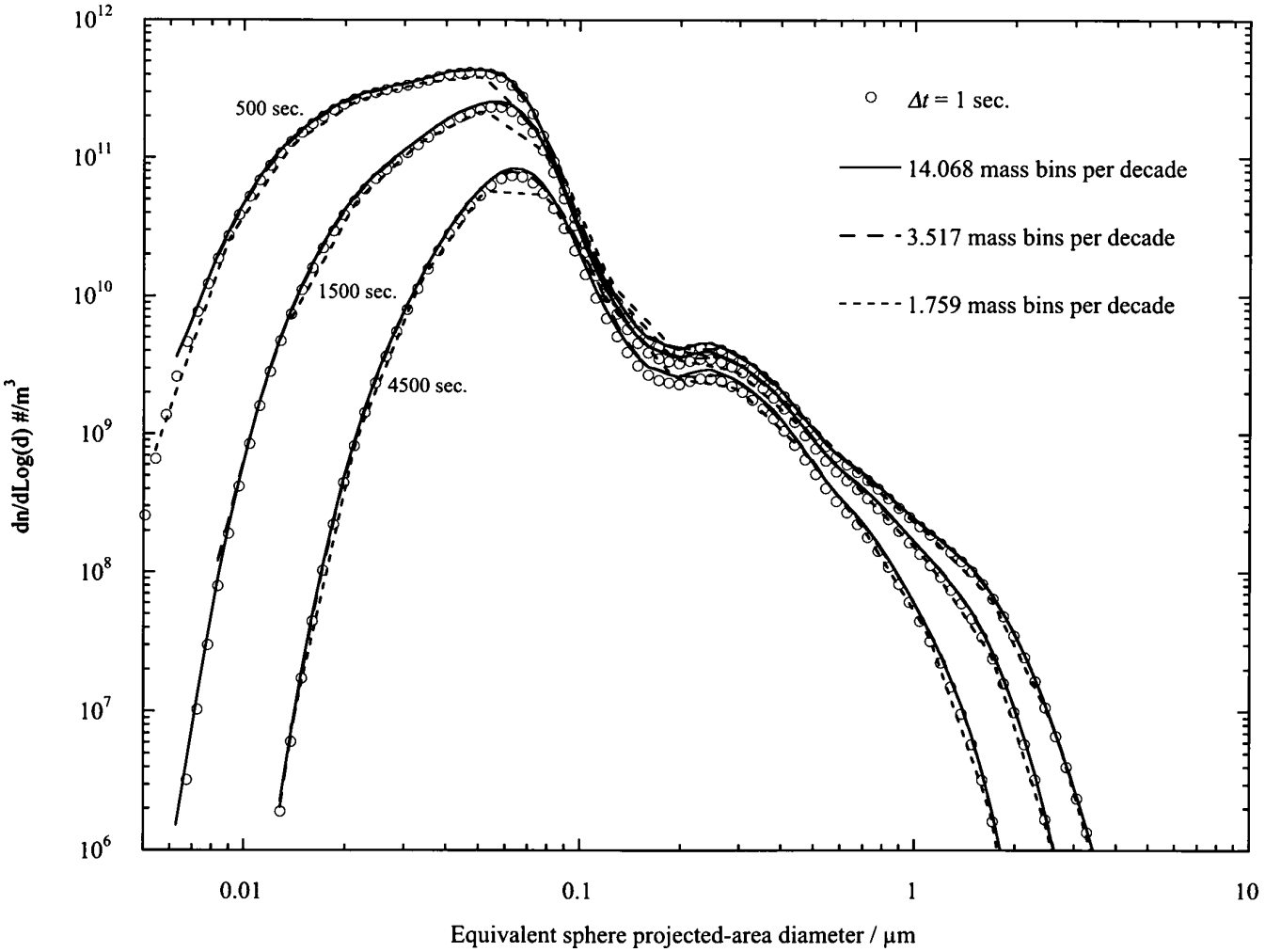

(b)

Figure 7. (Continued)

errors between evaluation points clearly increase with decreasing bins per decade (Figure 7b). Reducing the mass bins per decade to 1.759 (corresponding to 5.277 diameter bins per decade) represents a decrease in computation time of over 5000 times compared to the reference model.

The computational advantages in using a variable time step are demonstrated in Table 1, with an increase in computational speed of nearly two orders of magnitude being seen in this instance. Furthermore, qualitatively good agreement is seen with the reference distribution evolution using a value of n_{lim} as high as 5% (Figure 6). However, further improvements were seen in modeled distribution precision as n_{lim} reached 1%. Based on these data, subsequent runs of the model used $n_{lim} = 1\%$.

SUMMARY

The question of whether ultrafine particles generated into an environment with a broad polydisperse aerosol background will ultimately be inhaled as single particles or much larger agglomerates is most appropriately approached through numerical modeling. Comparisons between the model described here and a previously published analytical model of aerosol agglomeration has established good agreement with other codes for the simple case of a lognormal size distribution. Comparisons between the model and experimentally measured polydisperse distributions spanning more than three decades of particle diameter have established that the model is capable of closely predicting size distribution evolution with time for complex aerosols. Good agreement with experimental data in this case was dependent on estimates of constants affecting diffusion losses and gravitational settling, together with estimates of particle fractal dimension and primary particle diameter. Of these, the diffusion boundary layer is unlikely to be easily estimated in workplace situations without further work, and an extension of the model to a more complete treatment of gravitational and diffusional losses may be required. However, in situations where diffusion losses are not likely to be large and aerosols are well mixed, the model is well suited to estimating the relationship between the

size distribution of emitted ultrafine aerosols, and the aerosol that is ultimately inhaled.

REFERENCES

Baron, P. A., Sorensen, C. M., and Brockmann, J. E. (2001). Nonspherical Particle Measurements: Shape Factors, Fractals and Fibers. In *Aerosol Measurement. Principles, Techniques and Applications*, 2nd ed., edited by P. A. Baron and K. Willeke. Wiley Interscience, New York, pp. 705–749.

CEN (1993). *Workplace Atmospheres—Size Fraction Determination for Measurement of Airborne Particles*. Brussels, CEN.

Crump, J. G., Flagan, R. C., and Seinfeld, J. H. (1983). Particle Wall Loss Rates in Vessels, *Aerosol Sci. Tech.* 2:303–309.

Crump, J. G., and Seinfeld, J. H. (1981). Turbulent Deposition and Gravitational Sedimentation of an Aerosol in a Vessel of Arbitrary Shape, *J. Aerosol Sci.* 12(5):405–415.

Donaldson, K., Stone, V., Gilmore, P. S., Brown, D. M., and MacNee, W. (2000). Ultrafine Particles: Mechanisms of Lung Injury, *Phil. Trans. R. Soc. Lond. A* 358:2741–2749.

Forrest, S. R., and Witten Jr., T. A. (1979). Long-Range Correlations in Smoke-Particle Aggregates, *J. Phys. A Math. Gen.* 12:L109–L117.

Fuchs, N. A. (1964), *The Mechanics of Aerosols*. Oxford, Pergamon.

Gentry, J. W., and Cheng, S. H. (1996). The Effect of Special Classes of Collision Kernels on the Asymptotic Behavior of Aerosol Size Distributions Undergoing Coagulation, *J. Aerosol Sci.* 27(4):519–535.

Hagenloch, R., and Friedlander, S. K. (1989). Numerical Calculations of Collision Frequency of Molecules with DLA Clusters, *J. Colloid Interface Sci.* 133:185–191.

ISO (1995), *Air Quality—Particle Size Fraction Definitions for Health-Related Sampling*. Geneva, International Standards Organisation.

Jiang, Q., and Logan, B. E. (1991). Fractal Dimensions of Aggregates Determined from Steady State Size Distributions, *Environ. Sci. Technol.* 25:2031–2038.

Kinney, P. D., and Pui, D. Y. H. (1995). Inlet Efficiency Study for the TSI Aerodynamic Particle Sizer, *Part. Part. Syst. Charact.* 12:188–193.

Kommu, S., Khomami, B., and Biswas, P. (2003). Simulation of Aerosol Dynamics and Transport in Chemically Reacting Particulate Matter Laden Flows. Part I: Algorithm Development and Validation, *J. Aerosol Sci.* In Press.

Nemmar, A., Hoet, P. H. M., Vanquickenborne, B., Dinsdale, D., Thomeer, M., Hoylaerts, M. F., Vanbilloen, H., Mortelmans, L., and Nemery, B. (2002). Passage of Inhaled Particles into the Blood Circulation in Humans, *Circulation* 105:411–414.

Oberdörster, G. (2000). Toxicology of Ultrafine Particles: In Vivo Studies, *Phil. Trans. Roy. Soc. London Series A* 358(1775):2719–2740.

Otto, E., Fissan, H., Park, S. H., and Lee, K. W. (1999). The Log-Normal Size Distribution Theory of Brownian Aerosol Coagulation for the Entire Particle Size Range: Part II—Analytical Solution Using Dahneke's Coagulation Kernel, *J. Aerosol Sci.* 30(1):17–34.

Park, S. H., Lee, K. W., Otto, E., and Fissan, H. (1999). The Log-Normal Size Distribution Theory of Brownian Aerosol Coagulation for the Entire Particle Size Range: Part I—Analytical Solution Using the Harmonic Mean Coagulation Kernel, *J. Aerosol Sci.* 30(1):3–16.

Rogak, S. N., Flagan, R. C., and Nguyen, H. V. (1993). The Mobility and Structure of Aerosol Agglomerates, *Aerosol Sci. Technol.* 18(1):25–47.

Schmidt-Ott, A. (1988). In Situ Measurement of the Fractal Dimensionality of Ultrafine Aerosol-Particles, *Appl. Phys. Lett.* 52(12):954–956.

Seaton, A., MacNee, W., Donaldson, K., and Godden, D. (1995). Particulate Air Pollution and Acute Health Effects, *Lancet* 345:176–178.

Smoluchowski, M. V. (1917), *Z. Phys. Chem.* 92:129.

Vincent, J. H., and Clement, C. F. (2000). Ultrafine Particles in Workplace Atmospheres, *Phil. Trans. R. Soc. Lond. A* 358:2673–2682.

Wells, A. C., and Chamberlain, A. C. (1967), *Brit. J. Apply. Phys.* 18:1793.

Wu, M. K., and Friedlander, S. K. (1993). Enhanced Power-Law Agglomerate Growth in the Free-Molecule Regime, *J. Aerosol Sci.* 24(3):273–282.

Zimmer, A. T., and Maynard, A. D. (2002). Investigation of the Aerosols Produced by a High-Speed, Hand-Held Grinder Using Various Substrates, *Ann. Occup. Hyg.* 46(8):663–672.